GPS Ephemeris Verification for Local Area Augmentation System (LAAS) Ground Stations

Shuichi Matsumoto, *National Space Development Agency of Japan (NASDA)*
Sam Pullen and Mike Rotkowitz, *Dept. of Aeronautics and Astronautics, Stanford University*
Boris Pervan, *Dept. of Mechanical, Materials, and Aerospace Engineering, Illinois Institute of Technology*

ABSTRACT

Certain types of satellite failures, such as broadcast ephemeris messages that do not correspond to true satellite locations, can be difficult to detect by a Local Area Augmentation System (LAAS) ground facility (LGF) because satellites are observed from reference antennas that are very close together. Although ephemeris failures large enough to threaten LAAS user integrity should be very rare, a combination of monitors in the LGF is needed. This paper analyzes the combined effectiveness of several monitoring techniques and proposes solutions for all phases of LAAS operations.

The first solution is the combination of the GPS Operational Control Segment (OCS) and monitors included in the existing Category I LGF prototypes. Built-in LGF checks confirm that broadcast range and range-rate corrections have reasonable values and also compare computed satellite positions based on the current and previous ephemeris messages as well as the current almanac message. OCS monitoring by itself is insufficient for LAAS because OCS alerts are not guaranteed to meet the minimum time-to-alert requirement of 6 seconds for precision approaches. However, the combination of OCS and existing LGF monitoring is sufficient to meet the allocated per-approach probability of an undetected ephemeris error for Category I operations.

For Category II and III operations, the integrity requirement is 200 times tighter than for Category I; thus the monitors described above may be insufficient. This paper introduces new algorithms for validating ephemerides in three dimensions that can provide the needed improvement. The Differential Pseudorange Residual method (DPR) is used to detect ephemeris errors parallel to the LGF – satellite line of sight, and the Double Phase Difference with Ambiguity Search method (DPDAS) is used to detect ephemeris errors perpendicular to the line of sight (and thus very difficult to observe). Unlike RAIM, these two methods need only one other already-approved GPS satellite in view. These two methods can detect all ephemeris failures in three dimensions. This paper develops these algorithms in detail and presents experimental results from the Stanford LAAS Integrity Monitor Testbed (IMT).

1.0 Introduction: Threat from Ephemeris Errors

The Local Area Augmentation System (LAAS) will provide Global Positioning System (GPS) ranging corrections to users within the range of its VHF data broadcast (nominally 30 n.mi. but may be longer at altitude). LAAS will support precise, safe navigation that meets the requirements of Category I (and later Category III) aircraft precision approach [15]. Since corrections generated by the reference receivers of the LAAS Ground Facility (LGF) remove errors that are correlated between the LGF and user receivers, most errors that have their origin in the GPS satellites are removed when the user applies the LAAS correction. Satellite clock errors (such as those induced by Selective Availability, or SA) are very highly correlated because the same range error is present in LGF and user pseudoranges. However, errors in the reported location of the satellites (known as *ephemeris errors*) do not in general produce identical range errors – the error difference depends on the satellite-LGF-user geometry. For LGF-user separations under 30 n.mi. and nominal ephemeris errors (on the order of several meters), this error is negligible (less than 1 cm), but the possibility exists that very large ephemeris errors could produce hazardous user range errors.

1.1 Worst-Case User Errors due to Ephemeris Errors

The relationship between satellite ephemeris error and differential GPS (DGPS) user error is developed in detail in [1]. For a reference-to-satellite vector R, a reference-to-user vector δr, and a satellite ephemeris error vector δR relative to the broadcast satellite position, a user range error bound δE can be derived:

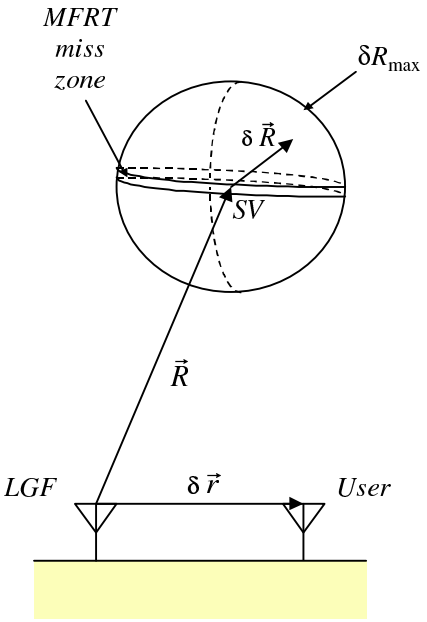

Figure 1: DGPS Ephemeris Error Geometry

$$\delta E \leq \frac{|\delta \vec{r}||\delta \vec{R}|}{|\vec{R}|} \quad (1)$$

The worst-case error results when δr is perpendicular to R and is also parallel to the ephemeris error δR. An example of such a situation would be an "in-track" ephemeris error (in the direction of the satellite's orbital motion) for a satellite directly above the LGF (at a 90° elevation angle) that happens to be parallel to the vector between the LGF and user. This worst-case error is clearly unlikely to occur, but it serves as a useful bound on the potential threat to LAAS users.

1.2 Probability of Large Satellite Ephemeris Errors

It is difficult to estimate the prior probability of a large satellite ephemeris error. No errors large enough to produce significant DGPS errors have been confirmed to date. A conservative estimate of this probability can be obtained from the GPS Standard Positioning Service (SPS) Signal Specification, which indicates that the probability of a "major service failure" shall be lower than 10^{-4} per hour per satellite [4]. This has been divided into six failure classes (including ephemeris failures), and the total failure probability has been evenly divided among them, giving an allocation to ephemeris failures of 1.67×10^{-5} per hour per SV [5]. This is conservative for ephemeris failures because they should form a small fraction of satellite failures (clock anomalies are much more common), but it is a reasonable point of departure.

Given an ephemeris failure, a missed-detection probability (P_{MD}) of 10^{-3} or below would reduce the resulting integrity risk to 6.94×10^{-10} per satellite per 150-second Cat. I approach, which translates into an undetected failure probability of 8.33×10^{-9} per approach for a maximum of 12 satellites in view. An allocation from the Cat. I signal-in-space (SIS) integrity risk limit of 2×10^{-7} per approach to ephemeris failures allows an undetected failure risk of 2.34×10^{-8} per approach [3]; thus some margin remains to allow higher P_{MD}'s.

1.3 User Range Errors that Threaten LAAS Integrity

The magnitude of user range errors that could lead to hazardous user position errors is derived in [2]. The vertical dimension of position error is the most limiting, and the largest vertical navigation sensor error that is presumed to not lead to unacceptable danger is known as the vertical alert limit (VAL). Based on a translation from the safety limits of existing Instrument Landing System (ILS) approaches, VAL has been set to be 10 meters for LAAS Cat. I and 5.3 meters for LAAS Cat. III precision approaches. Users determine if the navigation service is available by computing a vertical protection limit (VPL) and confirming that it is no greater than the VAL. VPL represents the size of the vertical position error under defined system states (nominal performance or single-reference-receiver failure) that is guaranteed to not be exceeded with a probability of one minus the defined signal-in-space integrity risk probability for that operation (2×10^{-7}/approach for LAAS Category I) [3].

VAL implicitly defines the worst GPS satellite geometry that is available for use – its vertical protection limit under nominal conditions equals the VAL. From this worst usable geometry and the standard deviation of the LGF pseudorange correction error, the ranging error that would cause VAL to be exceeded (all other satellites being nominal) can be approximated. This value, known as Minimum Acceptable Ranging Error (*MERR*), varies from 0.6 meters for high-elevation satellites to 2.7 meters for satellites at the 5-degree minimum elevation (based on the 'Class B3' LGF accuracy requirement) [2].

1.4 Maximum Acceptable Ephemeris Errors

Expression (1) in Section 1.1 can be rearranged to give the maximum acceptable ephemeris error (*MAEE*) as a function of *MERR* (or δE), LGF-user separation distance δr, and LGF-to-satellite distance $|\delta R|$:

$$MAEE = \frac{(MERR)(\delta \vec{R})}{|\delta \vec{r}|} \quad (2)$$

Figures 2 and 3 show the dependence of *MAEE* on LGF-user separation for a satellite at 90° elevation and on satellite elevation angle (upon which both *R* and *MERR* are dependent) for an LGF-user separation of 7.5 km, respectively. Note in Figure 2 that *MAEE* decreases

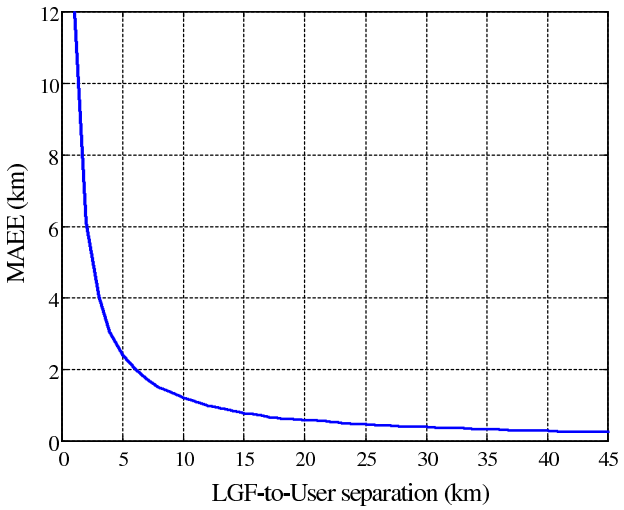

Figure 2: MAEE for Variable LGF-User Separation

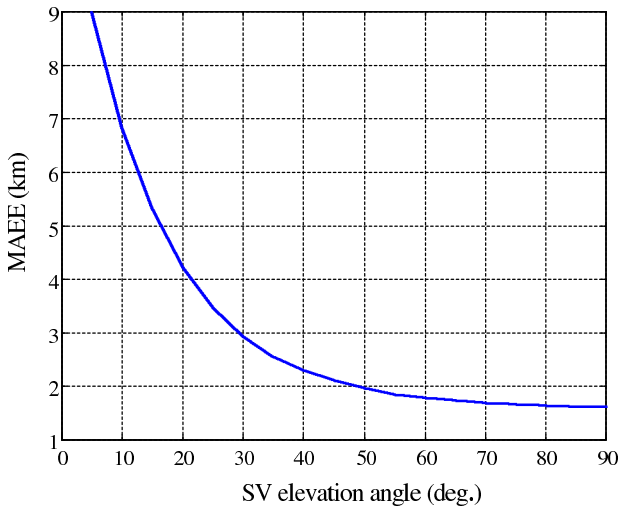

Figure 3: MAEE for Variable Satellite Elevation

rapidly as the user moves away from the LGF. The above *MERR*'s are the tightest values, which apply at an altitude of 200 ft above the approach threshold; thus the corresponding user locations are within 5-10 km of the LGF (depending on the airport layout). *MAEE* decreases rapidly as satellite elevation rises, since more weight is placed on high-elevation satellites in the position solution. Fortunately, satellites with large ephemeris errors are likely to be detected soon after they rise in view of the LGF, as will be demonstrated in Section 4.0.

2.0 Built-in LAAS Ephemeris Monitoring

A standard set of ephemeris monitors can be defined for Category I LAAS ground systems. This includes (1) steps that are built into the required processing of GPS measurements and the generation of DGPS corrections; (2) consistency checks of new ephemeris messages; and (3) checks of the magnitude of the DGPS corrections. LGF receivers automatically confirm that all requirements of the GPS SPS Interface Control Document (ICD) are met by each GPS satellite navigation message [4,6]. This includes checking that the navigation data message is not non-standard code (NSC: alternating '1's and '0's) and that satellite health bits and health-related bits in the Hand Over Word (HOW) and Preamble indicate that the data is good. Many satellite failures will automatically initiate NSC or other forms of invalid navigation data; thus alerting ground receivers immediately [7].

Uploads of new ephemeris data from the MCS normally occur once per day, and ephemeris changeovers usually occur every two hours (curve fits to satellite orbits are optimized for two-hour periods). The OCS only performs uploads when MS and GA visibility is guaranteed, and an OCS cross-check occurs after the upload, although MS/GA visibility is not guaranteed for subsequent changeovers [7]. After each changeover, the LGF compares the satellite locations given by the old and new ephemeris messages to confirm that the new ephemeris is consistent. A threshold of 250 meters is set on the 3-D satellite position difference, which is sufficient to guarantee integrity, although the difference under nominal conditions will be much smaller. When satellites first rise in view of the LGF, the prior ephemeris is not available to it, so the LGF instead compares the satellite positions between the new ephemeris and the latest almanac message. Since the almanac is much less accurate, the comparison threshold is set to be 7 km, but even this loose check is useful (it also will detect undesired lock on the cross-correlation of a different satellite).

Finally, each satellite pseudorange correction and correction rate to be broadcast by the LGF is checked to confirm that it lies within ± 327.67 m and ± 3.4 m/s, respectively. These limits represent not-to-exceed (NTE) values from the SPS Signal Specification [4] plus six times the normal one-sigma error with SA active (~25 m). The pseudorange limit is the same as the maximum correction that can be sent by the VDB, so this must be checked in any case. This is called the Message Field Range Test (MFRT), and it is effective because ephemeris errors greater than *MAEE* are very likely to have components in the satellite-to-LGF direction that are larger than 327 m. It is possible for satellites that fail MFRT at one time to pass it later while still causing hazardous errors; thus failing satellites should be removed from use for the duration of their pass overhead.

3.0 Operational Control Segment Probability Model

Since the performance of LAAS ephemeris monitoring is insufficient by itself to guarantee that the ephemeris-error integrity allocation is met, a study of the performance of the GPS Operational Control Segment (OCS) is needed to determine if the combination of

LAAS and OCS monitoring is sufficient. OCS headquarters is at the Master Control Station (MCS) in Colorado Springs, where all GPS maintenance decisions are made. The MCS is fed by a worldwide network of monitor stations (MS's), each with a GPS receiver that observes signals from all visible satellites. Uplinks from MCS to the satellites are transmitted by a network of ground antennas (GA's). Tables 1 and 2 show the locations of existing MS and GA sites as well as other sites that are planned to be incorporated into the OCS by 2001-02. These added sites will reduce the SV visibility gaps of the current OCS from 30% to 1% of the time [7].

Current Sites	Added NIMA Sites
Ascension Island	Adelaide, South Australia
Diego Garcia	Buenos Aires, Argentina
Kwajalein	Hermitage (London), Eng.
Kaena Pt, Hawaii	Manama, Bahrain
Schriever AFB, CO.	Quito, Ecuador
	USNO, Washington, D.C.
	(5 more sites under consideration)

Table 1: OCS Monitor Station (MS) Locations

Current Sites	Added AFSCN Sites
Ascension Island	Vandenberg AFB, CA.
Diego Garcia	New Boston Air Station, NH
Kwajalein	Oak Hangar, England
Cape Canaveral, FL.	Thule, Greenland
	Kaena Pt, Hawaii
	Andersen AFB, Guam
	Schriever AFB, CO.

Table 2: OCS Ground Antenna (GA) Locations

Based on the planned state of OCS in 2002 and later, a model of OCS ephemeris monitoring and alerting delay was constructed. The MCS L-band monitor provides updates to the MCS every 6 seconds based on differences between measured satellite-to-MS ranges and those computed based on the broadcast ephemeris and the known position of each MS. In addition, the residuals of the MCS Kalman Filter that is used to update satellite ephemeris and clock parameters are checked for unusual deviations every 15 minutes (at each filter update) [7,8]. Thresholds for these monitors have not been released by OCS. For this study, thresholds of 25 meters for the L-band monitor (in the satellite-to-MS direction) and 100 meters for the residuals check (in 3-D) are assumed.

When a satellite anomaly of significant size is detected by MCS, it issues a SATZAP to the affected satellite to change its PRN code to 37, which should not be tracked by user receivers [8]. The time interval between OCS

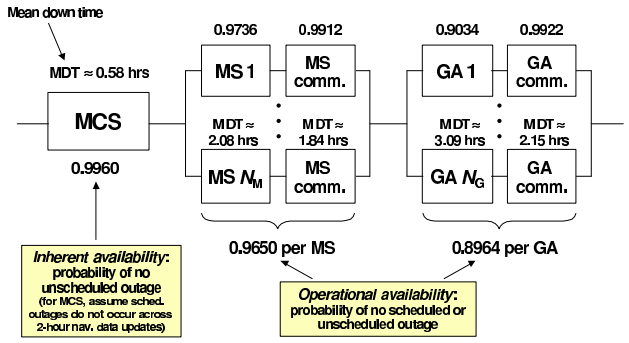

Figure 4: OCS Availability Model

alert and the SATZAP making the satellite unusable varies depending on operator workload and GA availability. Figure 4 shows a model of OCS component availability based on observed OCS performance as reported in the GOSPAR '96 report [9]. Individual MS and GA availability has been a significant limiting factor in the past, since often only one MS and/or one GA had visibility to a given GPS satellite. However, as NIMA and AFSCN sites are added to the OCS, multiple MS and GA visibility will be much more common. This redundancy will dramatically reduce the effect of a single MS or GA outage, leaving rare (and brief) MCS outages as the primary limiting factor on OCS availability.

The event tree shown in Figure 5 uses the model in Figure 4 to estimate the probabilities of various OCS monitor states for a typical GPS satellite. OCS is estimated to fully functional 98.4% of the time, meaning that MCS monitor violations (due to satellite failures) will be noticed right away, and only a nominal decision-making/communication delay will take place before the satellite is rendered unusable. OCS has not released any official statistics of these delays, but mode (most likely) delay estimates of 5 min. for the L-band monitor and 20 min. for the filter residuals check have been assumed in this study [7,8,9]. When OCS elements are non-functional or when MS or GA visibility is absent, mode added delay times apply based on the mean delay times (MDT's) in Figure 4 and the mean time before MS and

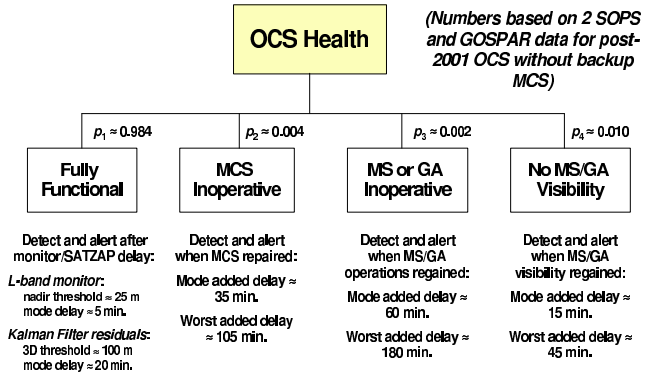

Figure 5: OCS Fault Detection Probability Tree

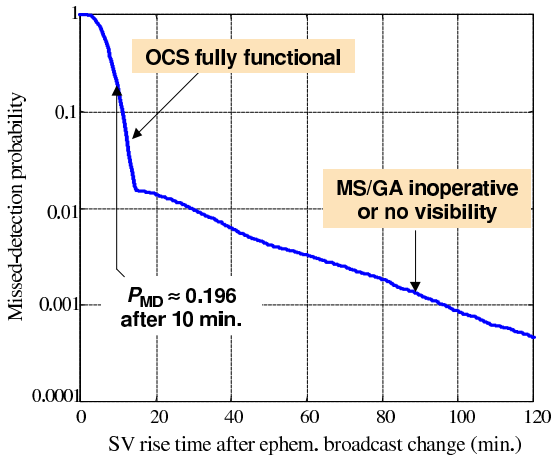

Figure 6: OCS P_{MD} for Class B Failures

GA visibility is expected to be restored. The MDT's are used to form triangular probability distributions of delay times (again, in lieu of better information) in which the minimum delay is one-third of the MDT and the maximum delay is three times the MDT.

4.0 Combined LAAS and OCS Effectiveness

In order to assess the combined ability of the LGF and OCS to detect ephemeris failures, two different sources of ephemeris errors large enough to threaten LAAS have been hypothesized. For *Class A* failures, the broadcast ephemeris becomes incorrect when the satellite performs an undesired maneuver from its nominal orbit. Multiple safeguards exist to prevent the uncommanded firing of GPS satellite thrusters (Block IIA satellites have two sets of 10 0.1-lb thrusters and two sets of two 1-lb thrusters); thus the probability of this occurring is very remote, but it cannot be completely discounted [7]. More likely (but still very rare) are *Class B* failures: those resulting from ephemeris broadcasts that do not represent the nominal satellite orbit. Some failure in the MCS processing and upload chain would be required to cause this.

4.1 Results for Class B Ephemeris Failures

Although OCS schedules daily satellite uploads when MS/GA visibility is assured, a subsequent ephemeris changeover could contain a Class B failure that is not immediately noticed. If the affected satellite then rises in view of an LGF site, the LGF is not guaranteed to detect it by the old-new ephemeris comparison. The OCS state probabilities and delay distributions from Section 3.0 have been combined via simulation to estimate the OCS missed-detection probability (the probability of OCS not rendering a satellite unusable before the satellite could be used by a LAAS site) in this case.

Figure 6 shows the resulting OCS missed detection probability as a function of satellite rise time (in view of the LGF) after an ephemeris changeover resulting in an erroneous satellite position. This plot has two segments. The first segment between 0-15 min. after ephemeris changeover has a rapidly-decreasing P_{MD} due to the effect of MCS monitoring when it is fully operational and has visibility to the failed satellite (~98.4% of the time). In this case, a SATZAP is guaranteed to take effect within 15 min. after the changeover (based on the distribution of SATZAP delays assumed in Section 3.0). For the approximately 1.6% of the time in which MCS does not have data for the affected satellite for one reason or another, alerting delays can be much longer and their distribution is much wider; thus P_{MD} decreases slowly beyond the 15-min. point. Since the distribution of time between satellite rise in view of the LGF and its most recent ephemeris changeover is uniformly distributed between 0 and 120 min. (for changeovers every 2 hours), the ensemble P_{MD} = 0.067. However, OCS may not sufficiently aid LAAS when a satellite rises shortly after an ephemeris changeover ($P_{MD} \cong 0.196$ after 10 min.).

An evaluation of LAAS monitoring effectiveness for Class B failures has been conducted based on the performance of the MFRT and ephemeris-almanac tests described in Section 2.0. As shown in Figure 1, the 3-D ephemeris error magnitude is assumed to be uniformly distributed between δR_{min} = 0 and δR_{max} = 30 km (the upper bound is conservative, as MFRT performance improves as the upper bound increases) and that the error direction is uniformly distributed. In this case, the probability that MFRT does not detect the error is equal to the ratio between (1) the volume of the thin cylinder in which the ephemeris error component in the direction of the LGF is under the MFRT threshold of PRC_{max} = 327 meters, and (2) the volume of the entire sphere:

$$P_{MD}(\text{MFRT}) \cong \frac{3PRC_{max}\left(\delta R_{max}^2 - \delta R_{min}^2\right)}{2\left(\delta R_{max}^3 - \delta R_{min}^3\right)} \cong 0.0049 \quad (3)$$

If the ephemeris error is missed by MFRT, it becomes hazardous to LAAS users only if the resulting user range error exceeds the MERR defined in Section 1.3. For an angle θ (assumed uniformly distributed between 0 and 360°) between the component of δR in the plane orthogonal to the satellite-user direction and the direction of δr in Figure 1, the error is hazardous when (see (2)) [1]:

$$\frac{\left|\delta\vec{R}\right|}{\sqrt{1.5}}\cos\theta \quad > \quad \frac{(MERR)\left|\vec{R}\right|}{\left|\delta\vec{r}\right|} \quad (4)$$

When the ephemeris-almanac check is added for the case of LGF approval of a newly-risen satellite, the relationship between δR and the LGF P_{MD} becomes complex; thus numerical integration is required. Figure 7 shows the result for *MERR* = 1.1 m, which is conservative for low-elevation satellites. LGF monitoring alone (MFRT

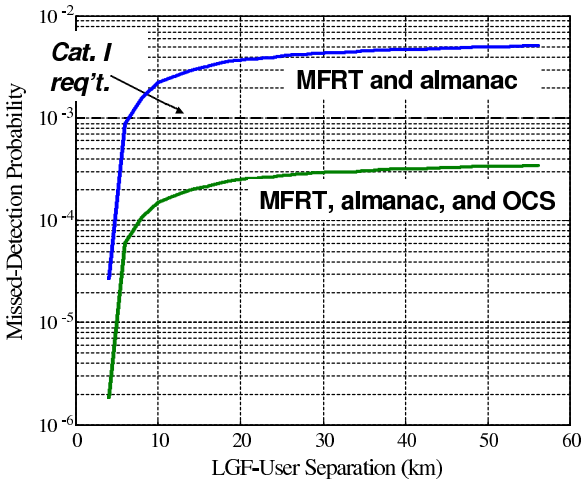

Figure 7: LAAS and Total P_{MD} for Class B Failures

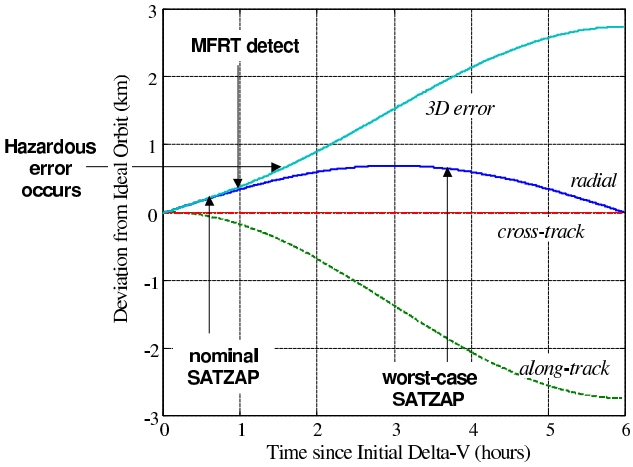

Figure 8: Result of Undesired Radial Thurst Impulse

and ephemeris–almanac checks) is sufficient to meet the P_{MD} requirement of 10^{-3} per satellite for LGF-user separations of 6 km or less, which will be the case for most Category I approaches. For larger separations, the addition of OCS monitoring gives ensemble P_{MD}'s that are more than sufficient to meet the requirement. From the rise-time-dependent OCS P_{MD}'s in Figure 6, an LGF "waiting time" requirement could be derived to cover any gap between the 10^{-3} requirement and the P_{MD} for LGF monitoring. However, the conservatism of both the OCS monitoring model and the P_{MD} requirement suggests that no waiting time after ephemeris changeover is needed for the LGF to approve satellites for Category I use.

4.2 Results for Class A Ephemeris Failures

In order to address the consequences of uncommanded satellite maneuvers, the Euler-Hill equations can be used to find the resulting satellite motions away from the nominal orbit described by the broadcast ephemeris [10]:

$$\begin{aligned} \ddot{x} - 2n\dot{y} - 3n^2x &= f_x \\ \ddot{y} + 2n\dot{x} &= f_y \\ \ddot{z} + n^2z &= f_z \end{aligned} \qquad (5)$$

where x, y, and z represent perturbations in the nadir, along-track, and cross-track directions from a nominal circular orbit with angular velocity n ($n \cong 1.454 \times 10^{-4}$ rad/s for GPS satellites), and f_x, f_y, and f_x are externally-applied forces per unit mass (the dry mass of a GPS satellite is about 804.6 kg). These equations can be solved for the zero-force case (after an impulsive thrust creates an initial perturbation rate) and the constant-force case (after a thruster gets stuck in the open position).

Figures 8 and 9 show the results for two uncommanded orbit deviation scenarios. In Figure 8, a 3-min. burst of a single 0.1-lb thruster is applied in the radial direction, causing an initial perturbation rate $\dot{x}_0 \cong 0.1$ m/s. In this case, the radial-axis component of the resulting ephemeris error is prominent; thus both the OCS L-band monitor and the LGF MFRT check detect this event well before the worst-case user error becomes hazardous (at *MAEE* ≅ 580 m). In Figure 9, a constant 0.1-lb force is applied in the along-track axis. The resulting along-track motion is harder for OCS and the LGF to detect. The OCS filter residuals check is the only monitor that detects the failure before the worst-case user error becomes hazardous, and the resulting SATZAP is not guaranteed to occur in time. Based on the SATZAP delay distributions derived in Section 3.0, the probability that the SATZAP does not take effect in time is about 0.016. This is the highest P_{MD} of any of the conceivable Class A failures studied, and while it is higher than the ensemble requirement of 10^{-3} for all ephemeris failures, it is acceptable because of the extreme rarity of this failure scenario [7].

5.0 Augmenting LAAS Ephemeris Monitoring

The results of the analyses in Section 4.0 suggest that the combination of OCS and LGF ephemeris monitoring of ephemeris errors is sufficient to meet the allocated

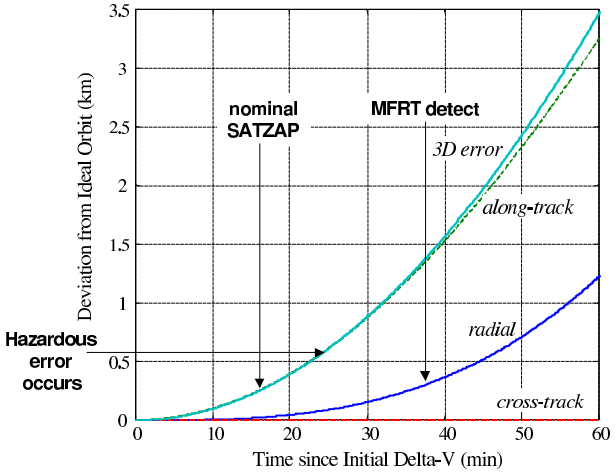

Figure 9: Result of Undesired Along-Track Thurst

integrity risk requirement for Category I LAAS precision approach. However, further ephemeris monitoring enhancements are useful both to provide an additional safety margin for Cat. I and to make it possible to meet the Category III integrity requirement, for which a P_{MD} on the order of 10^{-5} will be required (and the *MERR*'s are expected to tighten as well). One source of ephemeris information that will be readily available to all LAAS sites in CONUS is the use of Wide Area Augmentation System (WAAS) ephemeris corrections broadcast by geosynchronous satellites in a GPS-like L1 signal with a 250 bps data message [11]. Within the WAAS service volume, confirming that the δx, δy, δz satellite orbit corrections in WAAS Type 24 and 25 messages are no greater than ± 128 meters (the largest value that can be transmitted) insures that errors greater than the *MAEE*'s in Figures 2 and 3 will be detected. Since WAAS will flag such satellites as unhealthy in the Type 2 messages that are updated every 6 sec, checking Type 2 messages as well insures speedy LGF notification of any failures.

6.0 Enhanced Ephemeris Consistency Checking

In order to enhance the LAAS ephemeris monitoring to support Category II and III precision landing without reliance on WAAS, two new ephemeris monitoring approaches have been developed. The Differential Pseudorange Residual method (DPR) can detect ephemeris errors parallel to the LGF–satellite line of sight, and the Double Phase Difference with Ambiguity Search method (DPDAS) can detect ephemeris errors perpendicular to the line of sight. These methods go beyond the MFRT test described in Section 2.0 by checking the consistency between calculated and observed ranges across satellites visible to the LGF. Since only one other already-approved GPS satellite in view is required, there is no availability impact. The combination of these two methods with three GPS reference receivers can detect all sources of hazardous ephemeris failures in three dimensions. In this section, the algorithms of DPR and DPDAS are discussed in detail, and experimental results from the Stanford LAAS Integrity Monitoring Testbed (IMT) are presented.

6.1 Differential Psudorange Residual Method (DPR)

This method detects an ephemeris error parallel to the LGF–satellite line of sight by using a differential pseudorange residual. Its algorithm is shown below.

6.1.1 DPR Algorithm

For the DPR method, GPS pseudoranges to visible satellites are modeled as shown in (6) and (7):

$$\rho_1^{sat1} = |\mathbf{x}_1 - \mathbf{x}^{sat1}| + c \bullet b_1 + \delta\varepsilon_1^{sat1} + v_1^{sat1} \quad (6)$$

$$\rho_1^{sat2} = |\mathbf{x}_1 - \mathbf{x}^{sat2}| + c \bullet b_1 + \delta\varepsilon_1^{sat2} + v_1^{sat2} \quad (7)$$

where:

$\rho_i^{sat\,j}$: Pseudorange from satellite "j" received at LGF antenna "i"
$\mathbf{x}_i$: Position of LGF antenna "i"
$\mathbf{x}^{sat\,j}$: Position of GPS satellite "j"
$c \bullet b_1$: Range error due to LGF receiver "i" clock error
$\delta\varepsilon_i^{sat\,j}$: Range error caused by other error sources (SA, ionospheric delay, etc.)
$v_i^{sat\,j}$: LGF receiver measurement noise and multipath

The pseudorange residuals are calculated as follows:

$$e_1^{sat1} = \rho_1^{sat1} - |\mathbf{x}_1 - \mathbf{x}^{sat1}| = c \bullet b_1 + \delta\varepsilon_1^{sat1} + v_1^{sat1} \quad (8)$$

$$e_1^{sat2} = \rho_1^{sat2} - |\mathbf{x}_1 - \mathbf{x}^{sat2}| = c \bullet b_1 + \delta\varepsilon_1^{sat2} + v_1^{sat2} \quad (9)$$

Since the clock bias b_1 is same for all residuals, the differential pseudorange residual is given by:

$$\begin{aligned} de_1^{sat1,2} &= e_1^{sat1} - e_1^{sat2} \\ &= (PR_1^{sat1} - PR_1^{sat2}) - (|\mathbf{x}_1 - \mathbf{x}^{sat1}| - |\mathbf{x}_1 - \mathbf{x}^{sat2}|) \\ &= (\delta\varepsilon_1^{sat1} - \delta\varepsilon_1^{sat2}) + (v_1^{sat1} - v_1^{sat2}) \end{aligned} \quad (10)$$

As the standard deviation of SPS pseudorange error ($\delta\varepsilon_1^{sat1} + v_1^{sat1}$) is about 20.6 meters [13], the magnitude of the differential pseudorange residual can be limited at the 4.24σ level (Pr ~ $1\text{-}10^{-5}$) by the following DPR threshold:

$$|de_1^{sat1,2}| < 4.24 \times \sqrt{2} \times 20.6\,\text{m} \cong 123.6\,\text{m} \quad (11)$$

Although a slightly-larger estimate of the DPR threshold is derived from IMT data in Section 6.3, the value shown in (11) is used for the results in this section.

If there is a large error in the broadcast ephemeris, the differential pseudorange residual becomes:

$$\begin{aligned} d\tilde{e}_1^{sat1,2} &= (\rho_1^{sat1} - \rho_1^{sat2}) - (|\mathbf{x}_1 - \mathbf{x}^{sat1} - \delta\mathbf{x}^{sat1}| - |\mathbf{x}_1 - \mathbf{x}^{sat2}|) \\ &= de_1^{sat1,2} - \mathbf{1}_1^{sat1} \cdot \delta\mathbf{x}^{sat1} \end{aligned} \quad (12)$$

where:

$d\tilde{e}_1^{sat1,2}$: Differential pseudorange residual between satellites "1" and "2" with ephemeris error
$\delta\mathbf{x}^{sat1}$: Satellite position error caused by ephemeris error
$\mathbf{1}_1^{sat1} = \dfrac{(\mathbf{x}_1 - \mathbf{x}^{sat1})^T}{|\mathbf{x}_1 - \mathbf{x}^{sat1}|}$: LGF-satellite line-of-sight vector

Thus, GPS ephemeris errors parallel to the line of sight vector whose magnitudes are more than the threshold of 123.6 meters can be detected by the DPR test.

6.1.2 DPR Evaluation Results

To evaluate the DPR method, intentional ephemeris errors were added to the true ephemerides from a set of nominal GPS data collected by the IMT on Dec. 29, 1998. The results are shown in Figure 10. In this test, the *z* axis is parallel to the line of sight vector, the *y* axis is parallel to the orbital angular momentum vector of the GPS satellite, and the *x* axis is perpendicular to both the *y* and *z* axes. Figure 10 shows that a 250-meter error in the *z*-axis direction is easily detected.

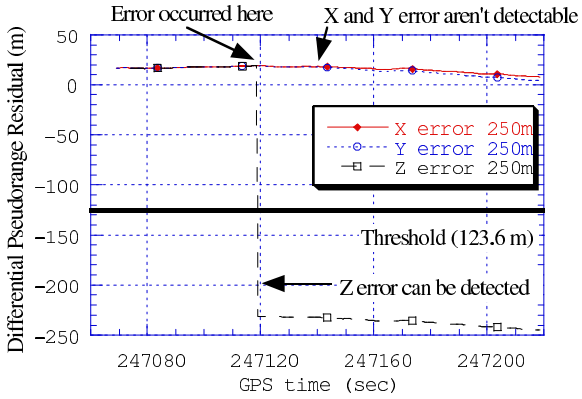

Figure 10: DPR Experimental Results

6.2 Double Phase Difference with Ambiguity Search Method (DPDAS)

As shown in Figure 10, the DPR method cannot detect satellite position errors perpendicular to the LGF-to-user line of sight vector. To detect perpendicular errors, the Double Phase Difference with Ambiguity Search method (DPDAS) has been developed.

6.2.1 DPDAS Algorithm

The DPDAS method uses LGF carrier phase measurements, which are modeled as follows:

$$\phi_i^{sat\,j} = |\mathbf{r}_i^{sat\,j}| + c \bullet b_i + \delta\varepsilon_i^{sat\,j} + m_i^{sat\,j} + I_i^{sat\,j} + v_i^{sat\,j} \qquad (13)$$

where:

$\phi_i^{sat\,j}$: Carrier phase from satellite "j" received at LGF antenna "i"

$\mathbf{r}_i^{sat\,j}$: Position vector from satellite "j" to LGF antenna

$c \bullet b_i$: Range error due to LGF receiver "i" clock error

$m_i^{sat\,j}$: Range error due to carrier phase multipath

$I_i^{sat\,j}$: Carrier phase integer ambiguity

$\delta\varepsilon_i^{sat\,j}$: Range error caused by other error sources (SA, ionospheric delay, etc.)

$v_i^{sat\,j}$: LGF receiver carrier phase noise

The carrier phase residual is given by:

$$e_i^{sat\,j} = \phi_i^{sat\,j} - |\mathbf{r}_i^{sat\,j}| = c \bullet b_i + \delta\varepsilon_i^{sat\,j} + m_i^{sat\,j} + I_i^{sat\,j} + v_i^{sat\,j} \qquad (14)$$

Since the clock bias b_i is same for all residuals, differencing the residual between two GPS satellites gives:

$$\begin{aligned} de_i^{sat\,1,2} &= e_i^{sat\,1} - e_i^{sat\,2} = (\phi_i^{sat\,1} - \phi_i^{sat\,2}) - (|\mathbf{r}_i^{sat\,1}| - |\mathbf{r}_i^{sat\,2}|) \\ &= (\delta\varepsilon_i^{sat\,1} - \delta\varepsilon_i^{sat\,2}) + (m_i^{sat\,1} - m_i^{sat\,2}) \\ &\quad + (I_i^{sat\,1} - I_i^{sat\,2}) + (v_i^{sat\,1} - v_i^{sat\,2}) \end{aligned} \qquad (15)$$

Since $\delta\varepsilon_i^{sat\,j}$, the range error caused by SA, ionospheric delay, etc., is almost the same for practical LGF antenna separations, taking a double phase difference between two GPS receivers removes these errors, giving:

$$\begin{aligned} d^2 e_{12}^{sat\,1,2} &= de_1^{sat\,1,2} - de_2^{sat\,1,2} \\ &= (\phi_1^{sat\,1} - \phi_2^{sat\,1}) - (\phi_1^{sat\,2} - \phi_2^{sat\,2}) \\ &\quad - (|\mathbf{r}_1^{sat\,1}| - |\mathbf{r}_2^{sat\,1}|) + (|\mathbf{r}_1^{sat\,2}| - |\mathbf{r}_2^{sat\,2}|) \\ &= (m_1^{sat\,1} - m_2^{sat\,1}) - (m_1^{sat\,2} - m_2^{sat\,2}) + (I_1^{sat\,1} - I_2^{sat\,1}) \\ &\quad - (I_1^{sat\,2} - I_2^{sat\,2}) + (v_1^{sat\,1} - v_2^{sat\,1}) - (v_1^{sat\,2} - v_2^{sat\,2}) \end{aligned} \qquad (16)$$

A triple phase difference (TPD) can eliminate the integer ambiguities, but this is not very helpful because the TPD eliminates ephemeris errors that occur before the affected satellite rises in view of the LGF. Figures 11 and 12 show the results of ephemeris error detection using the triple phase difference based on the IMT data collected on Dec. 29, 1998. Figure 12 shows that a simulated ephemeris error that occurs before the acquisition of the GPS signal cannot be detected by the triple phase difference method.

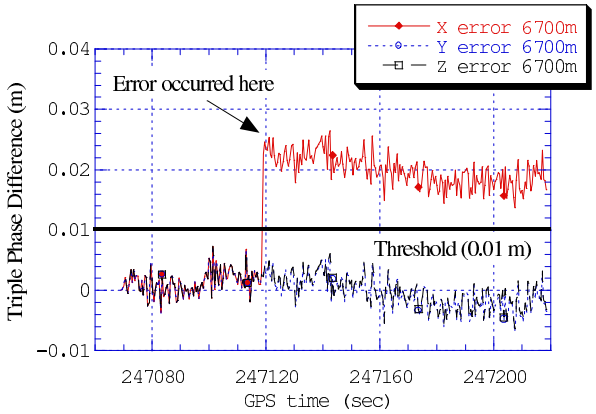

Figure 11: TPD Results (Error occurs in view)

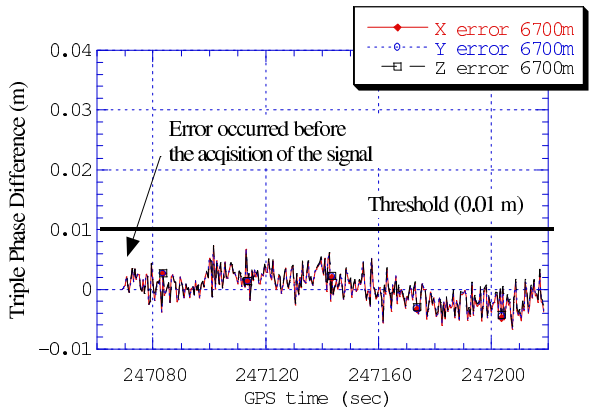

Figure 12: TPD Results
(Error occurs before LGF acquisition)

Thus a new approach, the Double Phase Difference with Ambiguity Search method (DPDAS), was developed. In this method, the double difference of the integer ambiguities in (16), $(I_1^{sat\,1} - I_2^{sat\,1}) - (I_1^{sat\,2} - I_2^{sat\,2})$, is found by an integer ambiguity search method before fault detection logic is applied. Since the integer ambiguity is normally bounded to within ± 5 meters by the pseudorange double difference and the search is only one-dimensional, only 52 candidates need to be checked to find the correct integer ambiguity. This method finds the integer ambiguity instantaneously and reliably because the 19-cm separation between integers is far larger than the remaining errors, such as carrier phase noise and multipath [16].

After estimating and removing the integer ambiguity from the double phase difference, the corrected double phase difference (CDPD) is obtained as follows:

$$\begin{aligned} d^2ec_{12}^{\,sat\,1,2} &= (\phi_1^{sat\,1} - \phi_2^{sat\,1}) - (\phi_1^{sat\,2} - \phi_2^{sat\,2}) - (|\mathbf{r}_1^{sat\,1}| - |\mathbf{r}_2^{sat\,1}|) \\ &\quad + (|\mathbf{r}_1^{sat\,2}| - |\mathbf{r}_2^{sat\,2}|) - (I_1^{sat\,1} - I_2^{sat\,1}) + (I_1^{sat\,2} - I_2^{sat\,2}) \\ &= (m_1^{sat\,1} - m_2^{sat\,1}) - (m_1^{sat\,2} - m_2^{sat\,2}) \\ &\quad + (v_1^{sat\,1} - v_2^{sat\,1}) - (v_1^{sat\,2} - v_2^{sat\,2}) \end{aligned} \tag{17}$$

If there is a satellite ephemeris error, the CDPD becomes:

$$\begin{aligned} d^2\tilde{e}c_{12}^{\,sat\,1,2} &= (\phi_1^{sat\,1} - \phi_2^{sat\,1}) - (\phi_1^{sat\,2} - \phi_2^{sat\,2}) \\ &\quad - (|\mathbf{r}_1^{sat\,1} - \delta\mathbf{x}^{sat\,1}| - |\mathbf{r}_2^{sat\,1} - \delta\mathbf{x}^{sat\,1}|) + (|\mathbf{r}_1^{sat\,2}| - |\mathbf{r}_2^{sat\,2}|) \\ &\quad - (I_1^{sat\,1} - I_2^{sat\,1}) + (I_1^{sat\,2} - I_2^{sat\,2}) \\ &= d^2ec_{12}^{\,sat\,1,2} - \{\mathbf{1}_1^{sat\,1} - \mathbf{1}_2^{sat\,1}\} \cdot \delta\mathbf{x}^{sat\,1} \\ &= (m_1^{sat\,1} - m_2^{sat\,1}) - (m_1^{sat\,2} - m_2^{sat\,2}) + (v_1^{sat\,1} - v_2^{sat\,1}) \\ &\quad - (v_1^{sat\,2} - v_2^{sat\,2}) - \{\mathbf{1}_1^{sat\,1} - \mathbf{1}_2^{sat\,1}\} \cdot \delta\mathbf{x}^{sat\,1} \end{aligned} \tag{18}$$

If the ephemeris error, $\{\mathbf{1}_1^{sat\,1} - \mathbf{1}_2^{sat\,1}\} \cdot \delta\mathbf{x}^{sat\,1}$, is large enough to be stand out from the carrier phase multipath error and receiver noise, this method can detect it.

The magnitude of multipath is dependent on the nature of the LGF reference receiver antennas and environment where they are sited. For DPDAS, it is essential to apply multipath mitigation techniques such as using Multipath Limiting Antennas (MLA's) in the LGF (this is planned for Cat. III LAAS ground stations) [15]. Another possibility is the using the Signal-To-Noise Ratio (SNR)-based multipath correction technique described in [14].

Using the SNR-based technique, for example, the typical multipath error is less than 6.8 mm at the 99.73% confidence level [14]. The noise error is 3 mm (RMS) according to a typical GPS receiver specification. If the noise error is normally distributed, the double difference of the noise, $(v_1^{sat\,1} - v_2^{sat\,1}) - (v_1^{sat\,2} - v_2^{sat\,2})$, has a 6-mm RMS. Since the CDPD is averaged for 5 seconds (or 10 samples) in the DPDAS program to smooth the noise, the error is reduced to about 2 mm (RMS). Combining these errors (assuming they are independent), a 4.2σ threshold (Pr ~ $1\text{-}10^{-5}$) for DPDAS can be set to 12.8 mm. The feasibility of this threshold is verified in the next section.

6.2.2 CDPD and GPS Satellite Position Error

The difference in the line-of-sight vectors between LGF reference receivers 1 and 2 in (18) is:

$$\begin{aligned} \mathbf{1}_1^{sat\,1} - \mathbf{1}_2^{sat\,1} &\cong \frac{-1}{|\mathbf{r}_1^{sat\,1}|}\{(\mathbf{1}_1^{sat\,1} \cdot \Delta\mathbf{x}) \cdot \mathbf{1}_1^{sat\,1} - \Delta\mathbf{x}\} \\ &= \frac{-1}{|\mathbf{r}_1^{sat\,1}|} \cdot \mathbf{p}_1^{sat\,1} \end{aligned} \tag{19}$$

where $\Delta\mathbf{x}$ is the baseline vector between LGF receiver antennas 1 and 2 (previously denoted as δr in Figure 1) and $\mathbf{p}_1^{sat\,1} = (\mathbf{1}_1^{sat\,1} \cdot \Delta\mathbf{x}) \cdot \mathbf{1}_1^{sat\,1} - \Delta\mathbf{x}$. The vector $\mathbf{p}_1^{sat\,1}$ is perpendicular to $\mathbf{1}_1^{sat\,1}$ as shown in Figure 13. Thus, DPDAS can observe GPS satellite position errors that are perpendicular to the LGF-to-satellite line-of-sight.

A further simplification is useful. Suppose ϕ is the angle between the error vector and the perpendicular

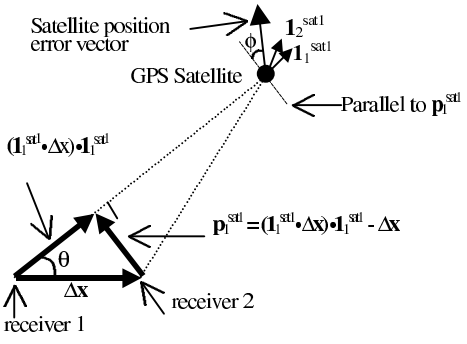

Figure 13: Relationship Between the Line-of-Sight Vector and the Perpendicular Vector

vector shown in Figure 13. In this case, (17) becomes:

$$d^2\tilde{e}c_{12}^{sat\,1,2} \cong d^2ec_{12}^{sat\,1,2} + \frac{|\Delta\mathbf{x}|\cdot\sin\theta\cdot\cos\phi}{|\mathbf{r}_1^{sat\,1}|}\cdot|\delta\mathbf{x}^{sat1}| \quad (20)$$

6.2.3 *Conditions Required for DPDAS*

For differential GPS navigation using pseudorange measurements, the observation equation is described by:

$$\begin{aligned}\Delta\rho &= (\rho_1^{sat1} - \rho_2^{sat1}) \\ &= (|\mathbf{r}_1^{sat1}| - |\mathbf{r}_2^{sat1}|) + c\cdot(b_1 - b_2) + (v_1^{sat1} - v_2^{sat1})\end{aligned} \quad (21)$$

Suppose antenna 1 is located at the LGF and antenna 2 is located at the user aircraft. If there is an ephemeris error on GPS satellite 1, (21) becomes:

$$\begin{aligned}\Delta\rho &= |\mathbf{r}_1^{sat1} - \delta\mathbf{x}^{sat1}| - |\mathbf{r}_{ac}^{sat1} - \delta\mathbf{x}^{sat1}| + c\cdot(b_1 - b_{ac}) + (v_1^{sat1} - v_{ac}^{sat1}) \\ &= \Delta\rho_0 - (\mathbf{1}_1^{sat1} - \mathbf{1}_{ac}^{sat1})\cdot\ \delta\mathbf{x}^{sat1} \\ &\cong \Delta\rho_0 + \frac{|\Delta\mathbf{x}_{1_ac}|\cdot\sin\theta\cdot\cos\phi_{ac}}{|\mathbf{r}_1^{sat\,1}|}\cdot|\delta\mathbf{x}^{sat1}|\end{aligned} \quad (22)$$

where:

$\Delta\rho_0$: Differential pseudorange without ephemeris error

$|\Delta\mathbf{x}_{1_ac}|$: Distance between LGF and aircraft

ϕ_{ac} : Angle between the error vector and the perpendicular vector at aircraft.

The last term of (22) is the aircraft position error in this scenario. Once the Minimum Acceptable Ranging Error (*MERR*) is determined for a certain distance between the LGF and airplane, the satellite position error that must be detected is determined such that:

$$\frac{|\Delta\mathbf{x}_{1_ac}|\cdot\sin\theta\cdot|\cos\phi_{ac}|}{|\mathbf{r}_1^{sat\,1}|}\cdot|\delta\mathbf{x}^{sat1}| > MERR \quad (23)$$

Since $|\cos\phi_{ac}| \le 1$:

$$|\mathbf{x}^{sat1}| > \frac{|\mathbf{r}_1^{sat1}|}{|\Delta\mathbf{x}_{1_ac}|\cdot\sin\theta}\cdot MERR = MAEE \quad (24)$$

The right-hand side of the inequality in (24) is the Maximum Acceptable Ephemeris Error (*MAEE*). From (20) and (23), the condition required for DPDAS to detect the ephemeris error is:

$$d^2\tilde{e}c_{12}^{sat\,1,2} > d^2ec_{12}^{sat\,1,2} + \frac{|\Delta\mathbf{x}|\cdot|\cos\phi|}{|\Delta\mathbf{x}_{1_ac}|\cdot|\cos\phi_{ac}|}\cdot MERR \quad (25)$$

In order to distinguish a significant ephemeris error from nominal multipath and receiver noise, $d^2ec_{12}^{sat\,1,2}$, the following condition must be met:

$$\frac{|\Delta\mathbf{x}|\cdot|\cos\phi|}{|\Delta\mathbf{x}_{1_ac}|}\cdot MERR > 2\cdot|d^2ec_{12}^{sat\,1,2}|_{\max} \quad (26)$$

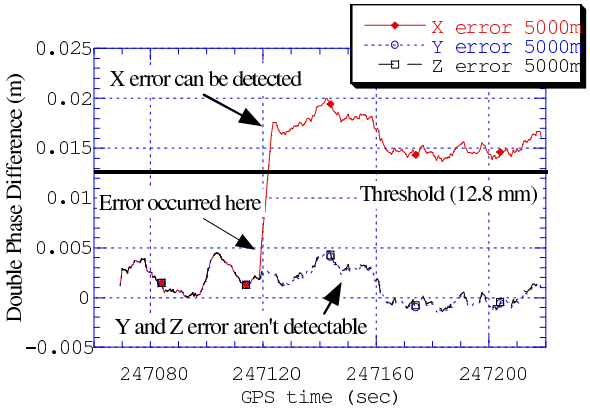

Figure 14: DPDAS Results (Error occurs in view)

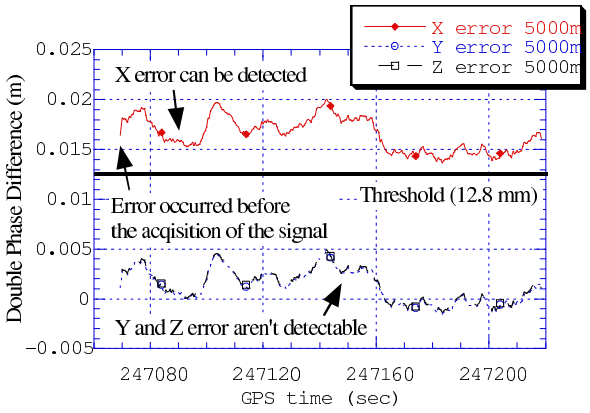

Figure 15: DPDAS Results (Error occurs before LGF acquisition)

Thus, the minimum antenna separation is given by:

$$\begin{aligned}|\Delta\mathbf{x}| &> 2\cdot|d^2ec_{12}^{sat\,1,2}|_{\max}\cdot\frac{|\Delta\mathbf{x}_{1_ac}|}{MERR\cdot|\cos\phi|} \\ &= \frac{2\cdot|d^2ec_{12}^{sat\,1,2}|\cdot|\mathbf{r}_1^{sat1}|}{\sin\theta\cdot|\cos\phi|\cdot MAEE}\end{aligned} \quad (27)$$

6.2.4 *Evaluation Results*

To test this method, intentional ephemeris errors were added to the IMT data collected on Dec. 12, 1998, and the DPDAS algorithm was applied. The following ephemeris error scenario was chosen:

(a) *MERR* = 2.7 m, *MAEE* = 5 km, $|\Delta\mathbf{x}_{1_ac}|$ = 7.5 km

(b) $d^2ec_{12}^{sat\,1,2}$ =12.8 mm (see Section 6.2.1)

(c) PRN 31, θ = 69°, ϕ=3°, $|\mathbf{r}_1^{sat1}|$ = 22,056 km

The results are shown in Figure 14. The definitions of the *x*, *y*, and *z*-axes are the same as those in Section 6.1. In this case, the GPS satellite whose velocity is parallel to the baseline vector ($\Delta\mathbf{x}$) between IMT antennas 2 and 3 (length = 72.3 m) is chosen. Figure 14 shows that a 5-km error in the *x* direction, which is perpendicular to the line of sight and is in the plane formed by the line-of-sight vector and the baseline vector, can be detected by

setting the threshold to 12.8 mm. For reference, Figure 15 shows the results of DPDAS when the ephemeris error occurs before the acquisition of the GPS signal. Unlike the triple difference method, DPDAS can detect the error.

6.3 Thresholds for DPR and DPDAS

This section examines the thresholds set for DPR and DPDAS under normal conditions based on data obtained from the LAAS Integrity Monitoring Testbed (IMT) at Stanford University on Dec. 29, 1998. The GPS satellite configuration and the relationship between the satellites and the ground antennas are shown in Figure 16.

PRN	Elev.	DPR μ, σ (m)	DPD #1 μ, σ (mm)	DPD #2 μ, σ (mm)	DPD #3 μ, σ (mm)
2	39°	84, 11	-1.5, 0.8	-0.1, 0.7	1.4, 0.9
3	16°	5.6, 5.9	11.1, 4.6	14.6, 2.9	3.4, 4.1
10	27°	63, 8	-1.0, 2.2	-0.1, 1.7	1.2, 3.1
13	60°	21, 11	1.2, 1.0	0.6, 1.1	-0.6, 2.0
18	51°	-3, 11	-4.5, 1.2	0.0, 0.9	4.6, 1.3
19	52°	40, 3	2.7, 0.6	0.1, 0.9	-2.6, 1.3
27	36°	-7, 10	1.1, 1.0	0.2, 1.2	-0.9, 1.7

Table 3: Nominal DPR and DPDAS Statistics

The results are shown in Table 3, where PRN 31 serves as the sole reference satellite for DPR and DPDAS calculations. For DPR, the largest $\mu + 3\sigma$ limit is 117 m for PRN 2. Allowing for some margin, the threshold for DPR can be set to 150 m. For DPDAS, the data from PRN 3 differs from that of the other visible satellites. Since PRN 3 was at low elevation (16°) and no multipath error mitigation technique was applied (beyond the use of standard choke-ring antennas), the carrier phase of PRN 3 most likely suffered from high multipath. The mitigation techniques discussed in Section 6.2.1, particularly the use of MLA's in the LGF, are needed to reduce the effect of multipath on low-elevation satellites to the same level as higher-elevation satellites. Excluding the data from PRN 3, the largest $\mu + 3\sigma$ limit is 8.5 mm for PRN 18. Applying a 25% margin, the DPDAS threshold can be set to 10.6 mm (approximately 3.75σ).

6.4 Three Dimensional Error Analyses

To further examine the combined capabilities of the DPR and DPDAS algorithms, a three-dimensional error analysis has conducted. The position errors in three orthogonal directions are individually added to the satellite position and DPR and DPDAS are applied to detect the satellite position errors. The position errors were set to 6700 m for the *x* and *y* axes and 250 m for the *z* axis. The IMT GPS antennas are located as shown in Figure 16. There are three baselines whose lengths are 20 m, 62.4 m, and 72.3 m, respectively. Since the two longer baselines point in almost the same direction and

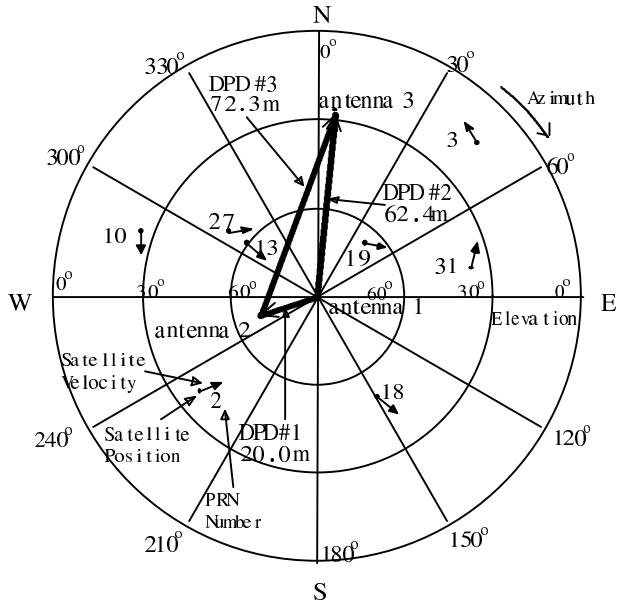

Figure 16: IMT GPS Satellite Locations (12/29/98)

the shorter baseline, DPD #1, is almost perpendicular to DPD #2, the existing IMT antenna configuration can only detect one ephemeris error dimension using DPDAS (because it is limited by the dimensions of the rooftop of the building it is on).

To summarize the results:

(a) DPR can detect all sizeable *z*-direction errors;
(b) DPDAS can detect either *x* or *y*-direction error:
- *x* error is detectable for PRN 10 and 31
- *y* error is detectable for PRN 2, 13, 18, 17, 27.

A better LGF antenna configuration uses two orthogonal baseline pairs 100 meters or more in length, as shown in Figure 17. In this case, DPDAS can detect GPS satellite position errors in both the *x* and *y* directions.

6.5 MERR and LGF Antenna Separations

The required baseline separations to support DPR and DPDAS monitoring can be derived based on the *MERR*'s for LAAS defined in Section 1.4. The minimum separation requirement for two antennas is given by (27). Since

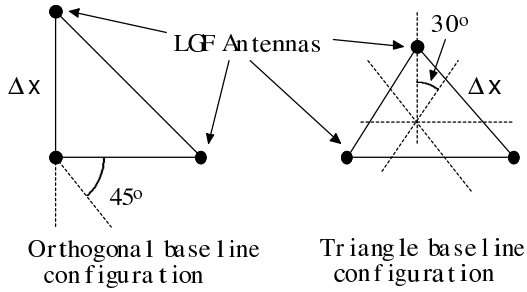

Figure 17: Preferred LGF Antenna Configurations

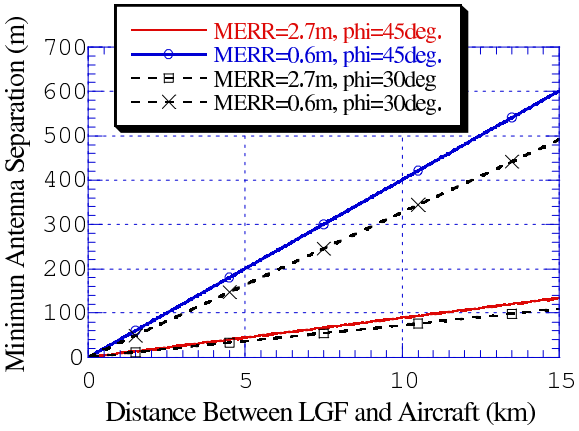

Figure 18: Minimum LGF Antenna Separation

$\left|d^2 e_{c12}^{sat1,2}\right|_{max}$ is 8.5 mm (3σ) in Section 6.3 and the maximum angle of the deviation from axes is 45 degrees on the orthogonal baseline configuration, the minimum antenna separation requirements is determined by the value of *MERR* and the LGF-user distance to which *MERR* applies. Figure 18 shows the relationship between *MERR* and the minimum antenna separation. On the same figure, the dotted lines show the relationship for the triangle antenna configuration shown in Figure 17, which slightly reduces the minimum separation required.

6.6 Application to Category III LAAS

Clearly, the DPR and DPDAS tests can significantly improve the effectiveness of LGF ephemeris monitoring. The sensitivity of DPR (to ephemeris errors parallel to the LGF-satellite line-of-sight) is similar to that of the existing MFRT check and can support a tighter threshold than MFRT uses (although MFRT can support a threshold tighter than the existing ± 327 meters based on Sections 6.1 and 6.3). Tightening this threshold would significantly improve the LGF P_{MD} for Class B failures beyond the result in Figure 7 of Section 4.1.

The DPDAS test is a more useful augmentation to LGF ephemeris monitoring because it is sensitive to satellite position errors perpendicular to the LGF-satellite vector, although its performance depends on the separation between LGF antennas as shown in Figure 18. The top two lines of Figure 18 apply to the tightest *MERR* for Category I approach, which applies to high-elevation satellites. For Category III approaches, values below 0.6 m are likely for high-elevation satellites, but larger values (between 0.6 and 2.7 m) are likely to apply to low-elevation satellites.

If DPDAS monitoring continues throughout the pass of each satellite, then the tightest *MERR*'s will apply, since monitoring will occur for low and high-elevation satellites. In addition, looser (~ 6σ) thresholds must be used because any loss of a satellite is a potential loss of continuity (which would cause all aircraft supported by that LGF to abort their precision approaches). Continuous monitoring does have the advantage of providing constant protection against Class A failures, which could occur at any time. Using multiple reference satellites (*N*-1 out of *N* satellites in view, instead of just one as shown in (17-18)) would reduce the threshold by a factor of $\sim\sqrt{N-1}$, but this introduces the complication of running DPDAS for each of *N* sets of *N*-1 reference satellites in order to identify which satellite has failed.

If the residual threat from Class A failures can be discounted, DPDAS is only needed to validate a satellite that has just risen, before it is approved for use. Once it is validated, the simpler old-new ephemeris test of Section 2.0 is adequate for subsequent ephemeris message changeovers. Thus, since DPDAS would be used for low-elevation satellites only, the applicable *MERR* is much higher. In addition, continuity is not risked because DPDAS will be completed before the LGF begins to broadcast corrections for newly-risen satellites. The resulting combination of higher *MERR* and tighter thresholds would significantly decrease the needed separation between LGF antennas.

Operationally, the key question to be answered for Category III LGF design is whether or not separations on the order of 100 meters (typical for Category I LGF antennas) will be sufficient. If DPDAS is only needed for newly-risen satellites, LGF-aircraft separations at the Category III decision height are no greater than 5 km or so, and low-elevation multipath error is similar to that that for higher satellites, separations of 100-200 meters may be sufficient. If larger LGF antenna separations are needed, far-field monitors (located near each runway threshold) that may be required to satisfy other LAAS Category III integrity requirements could also provide data to support long-baseline DPDAS monitoring.

7.0 Conclusions

Because Local Area Augmentation System Ground Facilities lack the ability to estimate GPS satellite orbit locations themselves, they are potentially vulnerable to large errors in the broadcast satellite ephemerides, even though these are expected to be very rare. A combination of LGF consistency checks and GPS Operational Control Segment satellite monitoring has been demonstrated to be sufficient to meet LAAS Category I integrity requirements with respect to both incorrect GPS navigation data and unplanned satellite maneuvers. However, such monitoring is not foolproof, thus use of

Wide Area Augmentation System corrections (where available) is desirable.

Although detailed requirements for LAAS Category III operations are not yet available, it is expected that additional ephemeris monitoring will be needed. Two new methods have been developed for this purpose. The DPR test (related to the MFRT test in Category I LAAS) is sensitive to ephemeris errors parallel to the LGF-satellite line-of-sight, while the DPDAS test is sensitive to ephemeris errors perpendicular to the line-of-sight that are difficult to detect otherwise. The addition of DPR and DPDAS to existing Category I LAAS monitoring is expected to meet Category III requirements, although longer separations between LGF reference antennas may become necessary.

Evaluation of the DPDAS algorithm will continue as part of the Stanford University Integrity Monitor Testbed in order to optimize the test procedure and its detection threshold. Once acceptable ranging errors and integrity allocations to satellite ephemeris failures are decided for Category III operations, the required separation between LGF reference antennas and/or far-field integrity monitors will be determined.

ACKNOWLEDGMENTS

The authors would like to thank 2 SOPS and Lawrence Cooper of ARINC for the detailed information on OCS operations that they provided. The comments of Ron Braff and JP Fernow of MITRE were also very helpful. The advice and interest of others in the Stanford GPS research group is appreciated, as is funding support from the FAA LAAS Program Office. The opinions discussed here are those of the authors and do not necessarily represent those of the FAA or other affiliated agencies.

REFERENCES

[1] B. Parkinson, P. Enge, "Differential GPS," in B. Parkinson and J. Spilker, Eds., *Global Positioning System: Theory and Applications*. Washington, D.C.: AIAA, 1996. Volume II, Chapter 1, pp. 3-50.

[2] C. Shively, "Acceptable Error Limits for Satellite Signal Faults in LAAS," *Proceedings of ION GPS-99*. Nashville, TN., Sept. 14-17, 1999 (forthcoming).

[3] *Minimum Aviation System Performance Standards for the Local Area Augmentation System*. Washington, D.C.: RTCA DO-245, September 28, 1998.

[4] *Global Positioning System Standard Positioning Service Signal Specification,* 2nd Edition, June 2, 1995. Internet site: http://www.navcen.uscg.mil/gps/geninfo/gpsdocuments/sigspec/

[5] R. Braff, "Estimation of SV Integrity Probabilities for the Cat. I LAAS Ground Facility," Version 4.0. McLean, VA.: The MITRE Corporation, Feb. 1999.

[6] *Navstar GPS Space Segment / Navigation User Interfaces* (ICD-GPS-200C). El Segundo, CA: ARINC, 25 September 1997. Internet Site: http://www.navcen.uscg.mil/gps/geninfo/gpsdocuments/icd200/

[7] S. Pullen, et.al., "Minutes of 2SOPS/FAA Interoperability Meeting." Colorado Springs, CO.: ARINC, Unpublished Manuscript, Feb. 3, 1999.

[8] J. Crum, R. Smetek, Jr., "Welcome to the Machine: An Overview of GPS Master Control Station Anomaly Detection and Resolution Techniques," *Navigation*. Vol. 44, No. 2, Summer 1997, pp. 133-152.

[9] *GPS OCS Performance Analysis and Reporting (GOSPAR) Project: Final Report.* Colorado Springs, CO.: Overlook Systems Tech., Ver. 2, Sept. 30, 1996.

[10] M. Kaplan, *Modern Spacecraft Dynamics and Control*. New York: John Wiley & Sons, 1976.

[11] P. Enge, *et.al*., "Wide Area Augmentation of the Global Positioning System," *Proceedings of the IEEE*. Vol. 84, No. 8, August 1996, pp. 1063-1089.

[12] *Minimum Operational Performance Standards for Global Positioning System/Wide Area Augmentation System Airborne Equipment*. Washington, D.C.: RTCA DO-229A, June 8, 1998.

[13] B. Parkinson, "GPS Error Analysis," in B. Parkinson and J. Spilker, Eds., *Global Positioning System: Theory and Applications*. Washington, D.C.: AIAA, 1996. Volume I, Chapter 11, pp. 469-483.

[14] P. Axelrad, C. Comp, P. MacDoran. "Use of Signal-To-Noise Ratio for Multipath Error Correction in GPS Differential Phase Measurements: Methodology and Experimental Results," *Proceedings of ION GPS-94*, Salt Lake City, Sept. 20-23, 1994, pp.655-666.

[15] R. Braff, "Description of the FAA's Local Area Augmentation System (LAAS)," *Navigation*. Vol. 44, No. 4, Winter 1997-1998, pp. 411-424.

[16] J. Jung, "High-Integrity Carrier Phase Navigation for Future LAAS using Multiple Civilian GPS Signals," *Proceedings of ION GPS-99*. Nashville, TN., Sept. 14-17, 1999 (forthcoming).